

Electron neutrino and antineutrino appearance in the full MINOS data sample

P. Adamson,⁸ I. Anghel,^{1,15} C. Backhouse,²¹ G. Barr,²¹ M. Bishai,³ A. Blake,⁵ G. J. Bock,⁸ D. Bogert,⁸ S. V. Cao,²⁹ D. Cherdack,³⁰ S. Childress,⁸ J. A. B. Coelho,^{30,6} L. Corwin,¹⁴ D. Cronin-Hennessy,¹⁸ J. K. de Jong,²¹ A. V. Devan,³² N. E. Devenish,²⁷ M. V. Diwan,³ C. O. Escobar,⁶ J. J. Evans,^{17,16} E. Falk,²⁷ G. J. Feldman,¹⁰ M. V. Frohne,¹¹ H. R. Gallagher,³⁰ R. A. Gomes,⁹ M. C. Goodman,¹ P. Gouffon,²⁴ N. Graf,¹³ R. Gran,¹⁹ K. Grzelak,³¹ A. Habig,¹⁹ S. R. Hahn,⁸ J. Hartnell,²⁷ R. Hatcher,⁸ A. Himmel,⁴ A. Holin,¹⁶ J. Hylen,⁸ G. M. Irwin,²⁶ Z. Ivan,^{3,22} D. E. Jaffe,³ C. James,⁸ D. Jensen,⁸ T. Kafka,³⁰ S. M. S. Kasahara,¹⁸ G. Koizumi,⁸ M. Kordosky,³² A. Kreymer,⁸ K. Lang,²⁹ J. Ling,³ P. J. Litchfield,^{18,23} P. Lucas,⁸ W. A. Mann,³⁰ M. L. Marshak,¹⁸ M. Mathis,³² N. Mayer,^{30,14} M. M. Medeiros,⁹ R. Mehdiyev,²⁹ J. R. Meier,¹⁸ M. D. Messier,¹⁴ D. G. Michael,^{4,*} W. H. Miller,¹⁸ S. R. Mishra,²⁵ S. Moed Sher,⁸ C. D. Moore,⁸ L. Muallem,⁴ J. Musser,¹⁴ D. Naples,²² J. K. Nelson,³² H. B. Newman,⁴ R. J. Nichol,¹⁶ J. A. Nowak,¹⁸ J. P. Ochoa-Ricoux,⁴ J. O'Connor,¹⁶ W. P. Oliver,³⁰ M. Orchanian,⁴ R. B. Pahlka,⁸ J. Paley,¹ R. B. Patterson,⁴ G. Pawloski,^{18,26} S. Phan-Budd,¹ R. K. Plunkett,⁸ X. Qiu,²⁶ A. Radovic,¹⁶ B. Rebel,⁸ C. Rosenfeld,²⁵ H. A. Rubin,¹³ M. C. Sanchez,^{15,1} J. Schneps,³⁰ A. Schreckenberger,¹⁸ P. Schreiner,¹ R. Sharma,⁸ A. Sousa,^{7,10} N. Tagg,²⁰ R. L. Talaga,¹ J. Thomas,¹⁶ M. A. Thomson,⁵ G. Tinti,²¹ R. Toner,^{10,5} D. Torretta,⁸ G. Tzanakos,² J. Urheim,¹⁴ P. Vahle,³² B. Viren,³ A. Weber,^{21,23} R. C. Webb,²⁸ C. White,¹³ L. Whitehead,^{12,3} S. G. Wojcicki,²⁶ T. Yang,²⁶ and R. Zwaska⁸

(The MINOS Collaboration)

¹Argonne National Laboratory, Argonne, Illinois 60439, USA

²Department of Physics, University of Athens, GR-15771 Athens, Greece

³Brookhaven National Laboratory, Upton, New York 11973, USA

⁴Lauritsen Laboratory, California Institute of Technology, Pasadena, California 91125, USA

⁵Cavendish Laboratory, University of Cambridge, Madingley Road, Cambridge CB3 0HE, United Kingdom

⁶Universidade Estadual de Campinas, IFGW-UNICAMP, CP 6165, 13083-970, Campinas, SP, Brazil

⁷Department of Physics, University of Cincinnati, Cincinnati, Ohio 45221, USA

⁸Fermi National Accelerator Laboratory, Batavia, Illinois 60510, USA

⁹Instituto de Física, Universidade Federal de Goiás, CP 131, 74001-970, Goiânia, GO, Brazil

¹⁰Department of Physics, Harvard University, Cambridge, Massachusetts 02138, USA

¹¹Holy Cross College, Notre Dame, Indiana 46556, USA

¹²Department of Physics, University of Houston, Houston, Texas 77204, USA

¹³Department of Physics, Illinois Institute of Technology, Chicago, Illinois 60616, USA

¹⁴Indiana University, Bloomington, Indiana 47405, USA

¹⁵Department of Physics and Astronomy, Iowa State University, Ames, Iowa 50011 USA

¹⁶Department of Physics and Astronomy, University College London, Gower Street, London WC1E 6BT, United Kingdom

¹⁷School of Physics and Astronomy, University of Manchester, Oxford Road, Manchester M13 9PL, United Kingdom

¹⁸University of Minnesota, Minneapolis, Minnesota 55455, USA

¹⁹Department of Physics, University of Minnesota Duluth, Duluth, Minnesota 55812, USA

²⁰Otterbein University, Westerville, Ohio 43081, USA

²¹Subdepartment of Particle Physics, University of Oxford, Oxford OX1 3RH, United Kingdom

²²Department of Physics and Astronomy, University of Pittsburgh, Pittsburgh, Pennsylvania 15260, USA

²³Rutherford Appleton Laboratory, Science and Technologies Facilities Council, OX11 0QX, United Kingdom

²⁴Instituto de Física, Universidade de São Paulo, CP 66318, 05315-970, São Paulo, SP, Brazil

²⁵Department of Physics and Astronomy, University of South Carolina, Columbia, South Carolina 29208, USA

²⁶Department of Physics, Stanford University, Stanford, California 94305, USA

²⁷Department of Physics and Astronomy, University of Sussex, Falmer, Brighton BN1 9QH, United Kingdom

²⁸Physics Department, Texas A&M University, College Station, Texas 77843, USA

²⁹Department of Physics, University of Texas at Austin, 1 University Station C1600, Austin, Texas 78712, USA

³⁰Physics Department, Tufts University, Medford, Massachusetts 02155, USA

³¹Department of Physics, University of Warsaw, Hoża 69, PL-00-681 Warsaw, Poland

³²Department of Physics, College of William & Mary, Williamsburg, Virginia 23187, USA

(Dated: October 30, 2018)

We report on ν_e and $\bar{\nu}_e$ appearance in ν_μ and $\bar{\nu}_\mu$ beams using the full MINOS data sample. The comparison of these ν_e and $\bar{\nu}_e$ appearance data at a 735 km baseline with θ_{13} measurements by reactor experiments probes δ , the θ_{23} octant degeneracy, and the mass hierarchy. This analysis is the first use of this technique and includes the first accelerator long-baseline search for $\bar{\nu}_\mu \rightarrow \bar{\nu}_e$. Our data disfavor 31% (5%) of the three-parameter space defined by δ , the octant of the θ_{23} , and the mass hierarchy at the 68% (90%) C.L. We measure a value of $2\sin^2(2\theta_{13})\sin^2(\theta_{23})$ that is consistent with reactor experiments.

The neutrino oscillation phenomenon is successfully modeled by a theory of massive neutrino eigenstates that are different from the neutrino flavor eigenstates. These sets of eigenstates are related by the PMNS matrix [1] which is commonly parameterized by three angles, θ_{ij} , and a CP-violating phase, δ .

The values of θ_{12} and θ_{23} have been measured [2–4] with indications that θ_{23} is not maximal [5–7]. The final angle, θ_{13} , is now known to have a nonzero value from measurements by reactor experiments [8–10], the measurement by the T2K [11] accelerator experiment, and from earlier MINOS results [12, 13].

Despite these accomplishments, the value of δ is still unknown, as is the ordering of the neutrino masses, which is referred to as the neutrino mass hierarchy. Much of the attention in the neutrino community is now focused on resolving these unknowns. The mass hierarchy is not only a fundamental property of neutrinos but also has a direct impact on the ability of neutrinoless double beta decay searches to state definitively whether the neutrino is its own antiparticle [14]. Reactor experiments make a pure measurement of θ_{13} , whereas the $\nu_\mu \rightarrow \nu_e$ and $\bar{\nu}_\mu \rightarrow \bar{\nu}_e$ appearance probabilities measured by accelerator experiments such as MINOS depend on the value of δ and $\sin^2(\theta_{23})$. In addition, the long-baseline of MINOS means that interactions between neutrinos and the matter of the Earth make the appearance probabilities dependent on the neutrino mass hierarchy [15, 16].

We report the result from the search for ν_e ($\bar{\nu}_e$) appearance in a ν_μ ($\bar{\nu}_\mu$) beam using the full MINOS data sample. This result uses an exposure of 10.6×10^{20} protons-on-target taken with a ν beam and an exposure of 3.3×10^{20} protons-on-target taken with a $\bar{\nu}$ beam. The neutrino sample is 30% larger than the sample used for the previous MINOS results on this topic [13]. This analysis represents the first long-baseline search for $\bar{\nu}_\mu \rightarrow \bar{\nu}_e$ appearance and places new constraints on θ_{13} and on a combination of δ , θ_{23} , and the neutrino mass hierarchy.

In the MINOS experiment [17], neutrino oscillation is studied with the NuMI beamline [18] by measuring neutrino interactions in two detectors. The Near Detector (ND), which has a fiducial mass of 29 tons, is at a distance of 1.04 km from the production target and is used to determine the composition of the beam before the neutrinos have oscillated. The Far Detector (FD), which has a fiducial mass of 3.8 kilotons, is at a distance of 735 km from the production target and is used to measure the change in the neutrino flavor composition of the beam. In both the ν and $\bar{\nu}$ beam modes, the NuMI beam has an energy spectrum that is peaked at 3 GeV. At the ND, the neutrino flavor composition of the neutrino interactions, as determined by a combination of simulation and measurement, is found to be 91.7% ν_μ , 7.0% $\bar{\nu}_\mu$, and 1.3%

ν_e and $\bar{\nu}_e$ for the ν beam mode and 58.1% ν_μ , 39.9% $\bar{\nu}_\mu$, and 2.0% ν_e and $\bar{\nu}_e$ for the $\bar{\nu}$ beam mode.

Both detectors are magnetized tracking calorimeters consisting of alternating planes of 2.54 cm thick steel and 1 cm thick scintillating plastic [17]. The scintillator planes are segmented into 4.1 cm wide strips with wavelength-shifting fibers embedded in the strips to collect light for readout by multi-anode photomultiplier tubes.

In the MINOS data sample, the flavor of a neutrino is determined only for charged-current (CC) interactions. ν_μ -CC and $\bar{\nu}_\mu$ -CC interactions are identified by the presence of a long muon track that extends beyond a cluster of energy depositions that are consistent with hadronic activity at the interaction vertex. Neutral-current (NC) interactions are identified by the energy depositions associated with hadronic activity. ν_e -CC and $\bar{\nu}_e$ -CC interactions produce an electromagnetic shower that typically leaves a compact cluster within 6 to 12 planes. This analysis does not distinguish between ν_e -CC and $\bar{\nu}_e$ -CC interactions.

The sample of events classified as ν_e -CC and $\bar{\nu}_e$ -CC interactions contains a background of interactions with similar topology as required for ν_e -CC and $\bar{\nu}_e$ -CC classification. NC interactions with a significant electromagnetic component and ν_μ -CC or $\bar{\nu}_\mu$ -CC interactions in which the muon track is not easily identified make up the majority of the background. Smaller contributions to the background arise from ν_τ -CC and $\bar{\nu}_\tau$ -CC interactions. In addition to backgrounds that mimic ν_e -CC and $\bar{\nu}_e$ -CC event topologies, intrinsic ν_e and $\bar{\nu}_e$ components of the NuMI beam must be taken into account.

Candidate ν_e -CC and $\bar{\nu}_e$ -CC events are required to fall within a fiducial volume and to be coincident in time and direction with the NuMI beam. We require the events to have shower-like topologies by rejecting events with tracks that are longer than 25 planes or extend more than 15 planes from a shower edge. In addition, reconstructed events must have at least five consecutive planes with deposited energy above a threshold; this threshold is defined as half of the energy deposited by a minimum ionizing particle. We require the events to have a reconstructed energy between 1 and 8 GeV where most of the ν_e and $\bar{\nu}_e$ appearance is expected.

We further classify the events in this pre-selected sample of shower-like events by using a library-event-matching (LEM) algorithm [19, 20]. Within the LEM algorithm, the topology of energy depositions that characterize the event is compared to a library of simulated signal and background events. Separate libraries are used for the events in the ν beam mode and $\bar{\nu}$ beam mode. The 50 best-matching events in the library are collected and used to produce three variables. These variables are the

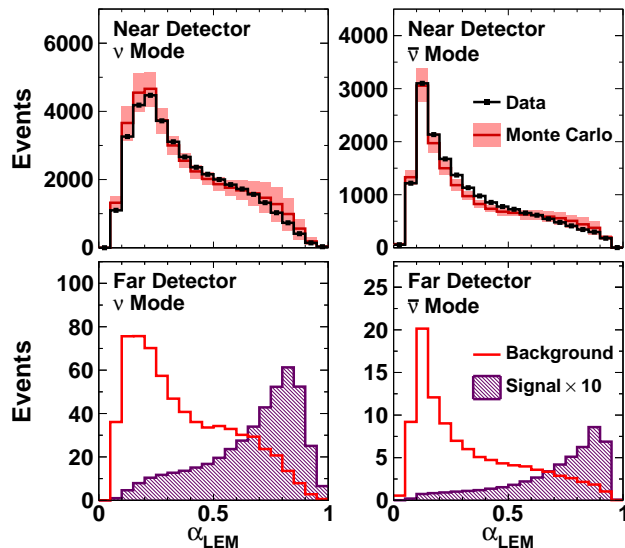


FIG. 1: Distributions of α_{LEM} . The plots in the left column correspond to the ν beam mode. The plots in the right column correspond to the $\bar{\nu}$ beam mode. The top row shows the distributions for ND selected events with a band about the simulation representing the systematic uncertainty. The bottom row shows the distributions for the predicted FD background and signal multiplied by 10 with $2\sin^2(2\theta_{13})\sin^2(\theta_{23}) = 0.1$, $\delta = 0$, and a normal mass hierarchy.

fraction of best-matching library events that are ν_e -CC or $\bar{\nu}_e$ -CC, the average inelasticity of the best-matching ν_e -CC or $\bar{\nu}_e$ -CC library events, and the average fraction of the energy depositions that overlap between the test event and the best-matching ν_e -CC or $\bar{\nu}_e$ -CC library events. These three variables and the reconstructed neutrino energy of the test event are then used as an input into an artificial neural network. The output value from the neural network is used to discriminate between signal and background events. This discriminant variable is referred to as α_{LEM} and is shown in Fig. 1. Signal events have a value near one, while background events cluster near zero. The maximum sensitivity to ν_e and $\bar{\nu}_e$ appearance is obtained by analyzing events with $\alpha_{LEM} > 0.6$.

Following the selection of ν_e -CC and $\bar{\nu}_e$ -CC candidate events, the ND data are used to study the rate of background from NC, ν_μ -CC and $\bar{\nu}_\mu$ -CC and intrinsic beam ν_e -CC and $\bar{\nu}_e$ -CC interactions. The NuMI beam can be tuned to produce different energy spectra. Among these different beam configurations, the relative contributions of the various backgrounds change in a well-understood way. By measuring the total of the three backgrounds in three different beam configurations, the relative amounts of the individual backgrounds can be deduced [21].

We use the measurement of the ND backgrounds to derive the FD background predictions for the data samples in the ν beam mode and in the $\bar{\nu}$ beam mode. For each sample, we divide simulated FD events into bins of energy

Systematic Effect	Uncertainty	
	ν mode	$\bar{\nu}$ mode
Energy Scale	2.7%	3.0%
Normalization	1.9%	1.9%
ν_τ cross-section	1.7%	2.0%
All Others	0.8%	2.5%
Total Systematic	3.8%	4.8%
Total Statistical	8.8%	23.9%

TABLE I: Systematic uncertainty on the FD background prediction for events with a value of $\alpha_{LEM} > 0.6$. Effects listed under “All Others” include the neutrino flux, cross sections, detector modeling, and background decomposition.

and α_{LEM} and correct each FD background component, bin-by-bin, by multiplying it by the measured ND ratio of data to simulated events for that background. Since the ND data sample does not contain ν_τ -CC and $\bar{\nu}_\tau$ -CC events from oscillation, we estimate the FD contribution from this small background component through simulation and a correction based on the observed ND ν_μ -CC and $\bar{\nu}_\mu$ -CC spectra.

The sources of systematic uncertainty that affect the background prediction are given in Table I. The effect of each source of uncertainty is evaluated by producing simulated ND and FD event samples that are modified according to the estimated size of each systematic effect. These modified samples are used to produce an altered FD background prediction for the systematic effect in question. We take the resulting difference between the nominal and modified prediction as the systematic uncertainty on the background prediction. The systematic effect that results in the largest reduction in sensitivity is a 2.0% uncertainty on the relative energy scale between the ND and FD.

With the absence of a ν_e -CC and $\bar{\nu}_e$ -CC signal in the ND, the signal selection efficiency cannot be extrapolated from the ND events in the same way as the background estimate. Therefore, to evaluate the signal efficiency, we select a sample of well identified ν_μ -CC events [22, 23], remove the energy depositions that are associated with the muon track [24], and insert the simulated energy depositions of an electron with an identical three-momentum [25]. This method effectively turns a well identified sample of ν_μ -CC and $\bar{\nu}_\mu$ -CC data events into a sample of ν_e -CC and $\bar{\nu}_e$ -CC data events. For the ν beam mode ($\bar{\nu}$ beam mode) data sample, we find the expected number of FD signal events with $\alpha_{LEM} > 0.6$ and the associated systematic uncertainty to be 33.7 ± 1.9 (3.9 ± 0.2) assuming $\sin^2(2\theta_{13}) = 0.1$, $\delta = 0$, $\theta_{23} = \pi/4$, and a normal mass hierarchy. This corresponds to an identification efficiency of $(57.4 \pm 2.8)\%$ for the ν beam mode and of $(63.3 \pm 3.1)\%$ for the $\bar{\nu}$ beam mode. The systematic uncertainties are evaluated in a way that is similar to the evaluation of the background systematics by using simulated samples that have been altered by a

Event Type	ν beam mode	$\bar{\nu}$ beam mode
NC	89.4	13.9
ν_μ -CC and $\bar{\nu}_\mu$ -CC	21.6	1.0
Intrinsic ν_e -CC and $\bar{\nu}_e$ -CC	11.9	1.8
ν_τ -CC and $\bar{\nu}_\tau$ -CC	4.8	0.8
$\nu_\mu \rightarrow \nu_e$ -CC	33.0	0.7
$\bar{\nu}_\mu \rightarrow \bar{\nu}_e$ -CC	0.7	3.2
Total	161.4	21.4
Data	152	20

TABLE II: Expected FD event yields for events with a value of $\alpha_{LEM} > 0.6$, assuming $\sin^2(2\theta_{13}) = 0.1$, $\delta = 0$, $\theta_{23} = \pi/4$, and a normal mass hierarchy.

systematic effect.

Events with $\alpha_{LEM} < 0.5$ are insensitive to ν_e and $\bar{\nu}_e$ appearance. These events are therefore used in a separate study to validate the analysis procedure. ND events with $\alpha_{LEM} < 0.5$ are used to predict FD event yields, which are found to agree with the FD data to within 0.3 (0.6) standard deviations of the statistical uncertainty for the data sample in the ν ($\bar{\nu}$) beam mode.

Events with $\alpha_{LEM} > 0.6$ are selected for further analysis in the ν beam mode and in the $\bar{\nu}$ beam mode. The expected and observed event counts in these samples are shown in Table II. The observed FD reconstructed energy spectra, in bins of α_{LEM} , are shown for the candidate events in Fig. 2. Assuming a three-flavor neutrino oscillation probability that includes matter effects [16], we simultaneously fit the data from the ν beam mode and $\bar{\nu}$ beam mode samples for the value of $2\sin^2(2\theta_{13})\sin^2(\theta_{23})$ while the value of the mass hierarchy and δ are held fixed. The fit is performed using the 15 bins formed by three bins of α_{LEM} and five bins of energy. This procedure is performed for all values of δ and both mass hierarchies, and the resulting confidence intervals, calculated using the Feldman-Cousins technique [26], are shown in Fig. 3. The values of the oscillation parameters used in the fit are taken from previous measurements [2, 4] and are set to $\sin^2(2\theta_{23}) = 0.957^{+0.035}_{-0.036}$, $|\Delta m_{32}^2| = (2.39^{+0.09}_{-0.10}) \times 10^{-3} \text{ eV}^2$, $\theta_{12} = 0.60 \pm 0.02$, and $\Delta m_{21}^2 = (7.59^{+0.19}_{-0.21}) \times 10^{-5} \text{ eV}^2$. The full set of statistical and systematic uncertainties on the prediction are taken into account when constructing the contours.

Assuming a normal mass hierarchy, $\delta = 0$, and $\theta_{23} < \pi/4$, we find that the data allow for values of $0.01 < 2\sin^2(2\theta_{13})\sin^2(\theta_{23}) < 0.12$ at 90% C.L. with the best-fit value of $2\sin^2(2\theta_{13})\sin^2(\theta_{23}) = 0.051^{+0.038}_{-0.030}$. Assuming an inverted mass hierarchy, $\delta = 0$, and $\theta_{23} < \pi/4$, we find that the data allow for values of $0.03 < 2\sin^2(2\theta_{13})\sin^2(\theta_{23}) < 0.18$ at 90% C.L. with the best-fit value of $2\sin^2(2\theta_{13})\sin^2(\theta_{23}) = 0.093^{+0.054}_{-0.049}$. The best-fit values show very weak dependence on the choice of octant for θ_{23} .

We are further able to place constraints on the

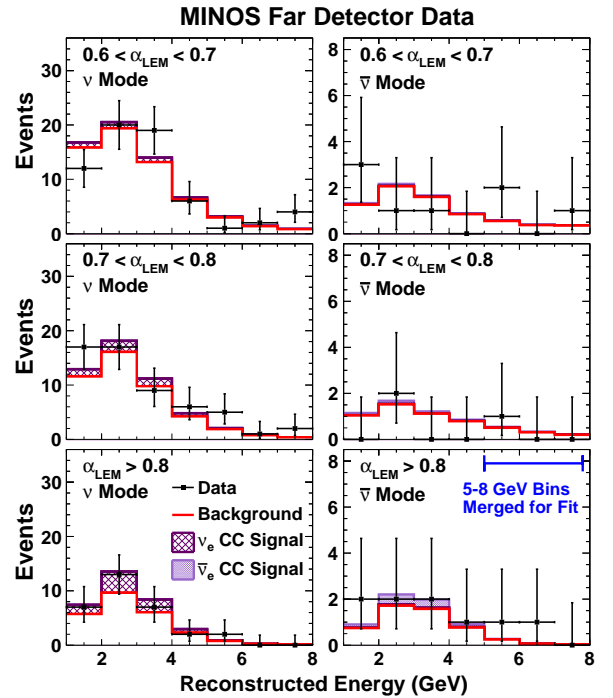


FIG. 2: The reconstructed energy distributions for three α_{LEM} ranges. The events with energy greater than 5 GeV are combined into a single bin for the fits. The vertical bars through the data points denote statistical uncertainties. The signal predictions assume $\sin^2(2\theta_{13}) = 0.051$, $\Delta m_{32}^2 > 0$, $\delta = 0$, and $\theta_{23} = \pi/4$. The plots in the left column correspond to data collected in the ν beam mode. The plots in the right column correspond to data collected in the $\bar{\nu}$ beam mode.

value of δ , the octant of θ_{23} , and the neutrino mass hierarchy by incorporating the current knowledge of $\sin^2(2\theta_{13}) = 0.098 \pm 0.013$ that we calculate from recent reactor data [8–10]. Fig. 4 shows the likelihood for our data as a function of δ for the four possible combinations of mass hierarchy and the octant of θ_{23} . The full set of statistical and systematic uncertainties on the prediction are taken into account when calculating the likelihood, as are the uncertainties on the oscillation parameters. This analysis represents the first result by a long-baseline experiment to use a combination of $\nu_\mu \rightarrow \nu_e$ and $\bar{\nu}_\mu \rightarrow \bar{\nu}_e$ appearance data, with external reactor constraints on θ_{13} , to probe δ , the θ_{23} octant degeneracy, and the mass hierarchy. Assuming $\theta_{23} > \pi/4$ ($\theta_{23} < \pi/4$), the data prefer an inverted hierarchy at 0.63 (0.04) units of $-\Delta \ln L$. Furthermore, as is indicated by the horizontal lines in Fig. 4, our data disfavor 31% (5%) of the three-parameter space defined by δ , the octant of the θ_{23} , and the mass hierarchy at the 68% (90%) C.L. This analysis demonstrates the potential discriminating power that can be achieved with the combination of reactor and $\nu_\mu \rightarrow \nu_e$ and $\bar{\nu}_\mu \rightarrow \bar{\nu}_e$ appearance data.

In conclusion, we have presented the results of ν_e and $\bar{\nu}_e$ appearance in ν_μ and $\bar{\nu}_\mu$ beams from the full MINOS

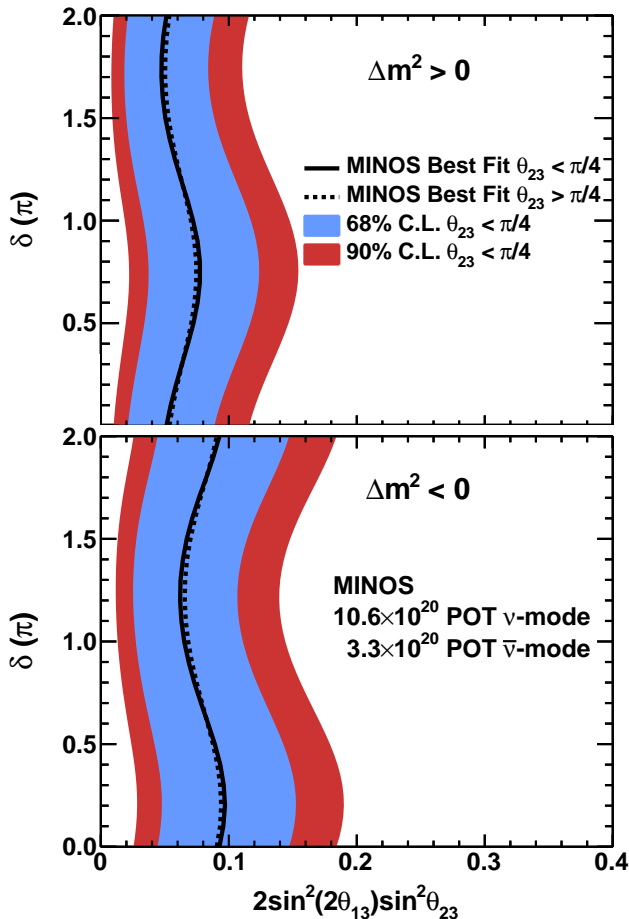


FIG. 3: The 68% and 90% confidence intervals of allowed values for $2\sin^2(2\theta_{13})\sin^2(\theta_{23})$ as a function of δ for the two mass hierarchies.

data sample. We have used these data to place new constraints on the mixing angle θ_{13} and have demonstrated how such data will be used in the future to break the degeneracy in the appearance probability created by the ambiguity in the octant of θ_{23} , the neutrino mass hierarchy, and the value of the CP-violating phase δ .

This work was supported by the US DOE; the UK STFC; the US NSF; the State and University of Minnesota; the University of Athens, Greece; and Brazil's FAPESP, CNPq, and CAPES. We are grateful to the Minnesota DNR, the crew of the Soudan Underground Laboratory, and the personnel of Fermilab for their contributions to this effort. We thank Texas Advanced Computing Center at The University of Texas at Austin for the provision of computing resources.

* Deceased.

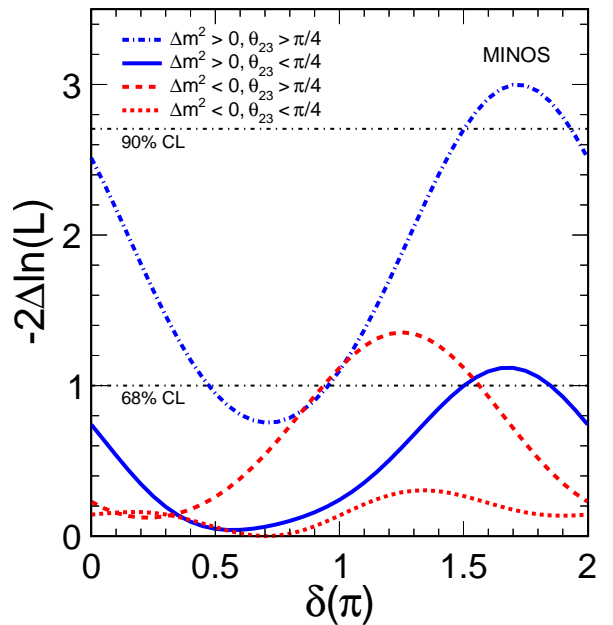


FIG. 4: The resulting values of the likelihood L , shown here as $-2\Delta\ln L$, from a fit of δ to our data using constraints from reactor experiments [8–10], assuming various values of the mass hierarchy and the sign of $\theta_{23} - \pi/4$. The difference is taken with respect to the best-fitting solution. Values above the horizontal dashed lines are disfavored at either 68% or 90% C.L.

- [1] B. Pontecorvo, JETP **34**, 172 (1958); V. N. Gribov and B. Pontecorvo, Phys. Lett. B **28**, 493 (1969); Z. Maki, M. Nakagawa, and S. Sakata, Prog. Theor. Phys. **28**, 870 (1962).
- [2] B. Aharmim *et al.* (SNO), Phys. Rev. Lett. **101**, 111301 (2008).
- [3] Y. Ashie *et al.* (Super-Kamiokande), Phys. Rev. D **71**, 112005 (2005).
- [4] R. Nichol, in *Proceedings of the XXV International Conference on Neutrino Physics and Astrophysics, Kyoto, Japan, June 2012* (to be published).
- [5] G. L. Fogli, E. Lisi, A. Marrone, D. Montanino, A. Palazzo, and A. M. Rotunno, Phys. Rev. D **86**, 013012 (2012).
- [6] M. C. Gonzalez-Garcia, Michele Maltoni, Jordi Salvado, and Thomas Schwetz, JHEP **12**, 123 (2012).
- [7] Y. Itow, in *Proceedings of the XXV International Conference on Neutrino Physics and Astrophysics, Kyoto, Japan, June 2012* (to be published).
- [8] Y. Abe *et al.* (Double Chooz), Phys. Rev. Lett. **108**, 131801 (2012).
- [9] F. P. An *et al.* (Daya Bay), Phys. Rev. Lett. **108**, 171803 (2012).
- [10] J. K. Ahn *et al.* (RENO), Phys. Rev. Lett. **108**, 191802 (2012).
- [11] K. Abe *et al.* (T2K), Phys. Rev. Lett. **107**, 041801 (2011).
- [12] P. Adamson *et al.* (MINOS), Phys. Rev. Lett. **103**, 261802 (2009); Phys. Rev. D **82**, 051102R (2010).

- [13] P. Adamson *et al.* (MINOS), Phys. Rev. Lett. **107**, 181802 (2011).
- [14] J. Beringer *et al.* (PDG), Phys. Rev. D **86**, 010001 (2012).
- [15] L. Wolfenstein, Phys. Rev. D **17**, 2369 (1978); S. P. Mikheyev and A. Yu. Smirnov, Sov. J. Nucl. Phys. **42**, 913 (1985).
- [16] E. K. Akhmedov *et al.*, J. High En. Phys. **04**, 078 (2004).
- [17] D. G. Michael *et al.* (MINOS), Nucl. Inst. & Meth. A **596**, 190 (2008).
- [18] K. Anderson *et al.*, FERMILAB-DESIGN-1998-01 (1998).
- [19] J. P. Ochoa, Ph.D. Thesis, California Institute of Technology, FERMILAB-THESIS-2009-44 (2009).
- [20] R. Toner, Ph.D. Thesis, University of Cambridge, FERMILAB-THESIS-2011-53 (2011).
- [21] J. A. B. Coelho, Ph.D. Thesis, Universidade Estadual de Campinas, FERMILAB-THESIS-2012-23 (2012).
- [22] R. Ospanov, Ph.D. Thesis, University of Texas at Austin, FERMILAB-THESIS-2008-04 (2008).
- [23] P. Adamson *et al.* (MINOS), Phys. Rev. Lett. **106**, 181801 (2011).
- [24] A. Holin, Ph.D. Thesis, University College London, FERMILAB-THESIS-2010-41 (2010).
- [25] J. Boehm, Ph.D. Thesis, Harvard University, FERMILAB-THESIS-2009-17 (2009).
- [26] G. J. Feldman and R. D. Cousins, Phys. Rev. D **57**, 3873 (1998).